

Real-time Outdoor Localization Using Radio Maps: A Deep Learning Approach

Çağkan Yapar[‡] Ron Levie[‡] Gitta Kutyniok^{†S} Giuseppe Caire[‡]

[‡] Institute of Telecommunication Systems, TU Berlin,

[‡] Faculty of Mathematics, Technion - Israel Institute of Technology,

[†] Department of Mathematics, LMU München,

^SDepartment of Physics and Technology, University of Tromsø

Abstract

This paper deals with the problem of localization in a cellular network in a dense urban scenario. Global Navigation Satellite Systems typically perform poorly in urban environments, where the likelihood of line-of-sight conditions between the devices and the satellites is low, and thus alternative localization methods are required for good accuracy. We present LocUNet: A fully convolutional, end-to-end trained neural network for the localization task, which merely depends on the received signal strengths (RSS) from Base Stations (BSs). In a wireless network, user devices scan the base station beacon slots and identify the few strongest base station signals for handover and user-base station association purposes. In the proposed method, the user to be localized simply reports such received signal strengths to a central processing unit, which may be located in the cloud. Alternatively, the localization can be performed locally at the user. Using the pathloss radio map estimations and the RSS measurements, LocUNet can localize users with state-of-the-art accuracy and enjoys high robustness to inaccuracies in the estimations of the radio maps. The proposed method does not require pre-sampling of the environment; and is suitable for real-time applications, thanks to the RadioUNet, a neural network-based radio map estimator. Moreover, two novel datasets that allow for numerical evaluations of RSS and ToA methods in realistic urban environments are presented and set publicly available for the use of research community. By using these datasets, we also provided a fair comparison of state-of-the-art RSS and ToA-based methods in the dense urban scenario, LocUNet outperforming all the compared methods.

Index Terms

localization, radio map, pathloss, deep learning, dataset.

I. INTRODUCTION

The location information of a User Equipment (UE) is essential for many current and envisioned applications that range from emergency 911 services [1], autonomous driving [2], intelligent transportation systems [3], proof of witness presence [4], 5G networks [5], to social networks, asset tracking and advertising [6], to name some.

In urban environments, Global Navigation Satellite Systems (GNSS) alone may fail to provide a reliable localization estimate due to the lack of line-of-sight conditions between the UE and the GNSS satellites [7]. In addition, the continuous reception and detection of GNSS signals is one of the dominating factors in battery consumption for hand-held devices. It is thus necessary to resort to other complementary means to achieve the UE localization with the desired high accuracy. In cellular networks, the position of UE can be estimated by using different metrics that UE may report or the network can infer. The most prominent localization methods in the literature are based on Time of Arrival (ToA) [8], [9], Time Difference of Arrival (TDoA) [10], Angle of Arrival (AoA) [11] and Received Signal Strength (RSS) [12] measurements.

A. Received Signal Strength (RSS)

Received signal strength quantifies the received power (averaged over a limited time interval of the beacon frames and over the signal bandwidth; hence, it is not subject to small scale fluctuations, and coherent reception is not necessary) at a UE due to signals sent by a (anchor) Base Station (BS). Since the transmit power of the BS on its beacon signal slots is fixed and known, the received signal strength is a function of the pathloss of the propagation between the BS and the UE. In fact, received signal strength measurements of beacon signals are routinely performed by UEs and reported to the system as “received signal strength indicators” (RSSI). Reporting RSS information is a standard feature in most current wireless protocols. For example, this is used to trigger handovers and to enable UE-BS association for load balancing purposes. Therefore, exploiting RSS information for localization is attractive since it is a feature already built-in in the wireless protocols and does not require any further specific hardware at the UE, whereas the time-based (ToA and TDoA) and angle-based (AoA) methods require high precision clocks and antenna arrays, respectively [13], [14].

Remark 1: For ease of exposition, throughout the paper we consider a cellular network scenario with BSs. Essentially, any wireless signal source with known location, e.g., WiFi-Hotspots, can be utilized.

B. Ranging-Based Methods

In ranging-based techniques, the distances between the UE and the BSs are used to estimate the position of UE by lateration. Here, the distances are estimated by using RSS or ToA measurements, based on a statistical signal attenuation or time delay model to estimate the distance between the UE and the BS. However, using such models is not appropriate in urban settings, since in practice the signal undergoes diverse propagation phenomena such as penetrations, reflections, diffractions, and wave guiding effects, due to the presence of obstacles in the environment. This leads to very large errors in the distance estimation (See Remark 2 and [15]). We call this phenomenon *range estimation mismatch*. Several works [8], [9], [16]–[23] proposed methods to mitigate the effects of obstructions in the range estimation mismatch. Nevertheless, these methods do not directly use a complete model of the propagation phenomena, and only partially alleviate the aforementioned problem.

C. Fingerprint-Based Methods

Fingerprint-based methods, as opposed to ranging-based methods, do not impose any modeling assumption on the signal strength propagation. Instead, these methods rely on offline generated extensive databases of the measured signatures of the signal at different locations. Given a reported signal fingerprint, these methods infer the location of the UE by “looking up” a location with a similar fingerprint from the database (radio map, cf. Section II-A). Many fingerprint types, such as visual, radio wave (e.g. RSS or the baseband transfer function with complex channel coefficients, i.e., the so-called Channel State Information (CSI)), or motion fingerprints, can be utilized for localization purpose [24]. In this paper we focus on RSS signatures, which are more robust to changes in the propagation environment and much more lower dimensional than CSI signatures. Fingerprint-based methods are well-known for outperforming the ranging-based techniques in complex urban environments [25]. Many machine learning techniques based on RSS fingerprints have been applied for positioning in past work, e.g. [26].

D. Physical Simulations of Radio Maps and RadioUNet

A major drawback of fingerprinting is the difficulty in generating and updating the radio maps. Fingerprinting requires a labor intensive, time consuming and expensive site surveying to generate the radio maps, which needs to be repeated as the environment changes. Hence, numerous methods have been proposed to reduce the site surveying efforts (See e.g. [27], [28]).

A more feasible alternative for generating the radio map is using physical simulation methods such as ray-tracing [29]–[31], thereby bypassing the extensive measurement campaigns. Based on an approximate model of the physical signal propagation phenomena, such simulations yield very accurate predictions, especially when accurate geometrical description of the urban environment is available. Many previous works proposed using simulated radio maps for localization, e.g. [26], [32]–[39].

However, such simulations are computationally demanding and are thus not suitable for real time applications. Recently, an efficient deep learning-based method termed *RadioUNet* [40] (see Subsection II-C) was proposed by the authors of this paper. This algorithm enables the generation of high accuracy pathloss radio maps in much shorter time, and is thus adopted as an important building block of the current work.

E. Machine Learning For Localization

Lately, several machine learning-based localization approaches have been proposed, e.g. [41]–[43], see the recent surveys [44], [45]. To the best of our knowledge, none of the previous works benefited from the availability of accurate radio maps via physical simulations (or good approximations like *RadioUNet*), and relied solely on the RSS/CSI measurements of the signals from the BSs at the UE, or vice versa. We note that the radio maps serve straightforwardly as a means to assess a likelihood for the location of the UE, for each BS, e.g., by simply comparing the reported RSS with the radio map estimate at the location at question.

As opposed to the previous work, *LocUNet* does not require any RSS/CSI samples and training when deployed in a new environment. Moreover, *LocUNet* fully utilizes radio map estimations (See Section III) thanks to its fully-convolutional design (cf. Remark 7).

Remark 2: *It should be noticed here that there exist plenty of pathloss statistical models which are routinely used in standardization (e.g., 3GPP) for different propagation environments. These models consider the pathloss as a random variable whose mean (in dB scale) follows typically a piece-wise linear decreasing function of distance, and the fluctuations around the mean are Gaussian in dB scale, yielding the classical log-normal shadowing. These models are obtained by pooling a large number of measurements and plotting the signal strength in dB scale versus distance. Hence, their radial symmetry (i.e. the pathloss statistics are a function of the distance between Tx and Rx only) is a built-in feature of the modeling itself. Unfortunately, this is far from realistic for any specific urban environment, characterized by given building shapes and locations*

and street canyon propagation. We would like to stress here that a key difference between our proposed method and other RSS-based methods is that we use an accurately learned pathloss model (using RadioUNet), which reflects the specific non-radial characteristics of a given specific environment. On the other hand, our approach is also very different from other Deep Learning approaches that require that radio signatures are collected on a dense grid of locations for any specific environment. In fact, the only required input to RadioUNet is the city map and the location of the BS transmitters, which are as a matter of course accurately known by the system. No signatures must be collected for the specific environment in a system setup phase. As a matter of course, even with the very accurate pathloss models, mismatches between the estimations and true pathloss measurements are inevitable, due to the changes in the environment in a urban setting. As we shall see later, LocUNet can also deal with such inaccuracies.

F. State-of-the-Art Urban Localization in Current Commercial Use

The industry state-of-the-art on radio localization as implemented by systems such as Google Maps and Apple Maps are based on a multitude of sensor data, including GNSS, “radio signatures” of all sort (e.g., WiFi SSIDs, cellular channel quality, detailed channel frequency response of the fading channels over the OFDM subcarriers, and so on), and these data are fused via some machine learning scheme. Since these practical implementations are ad-hoc industry intellectual property and not revealed in the open literature at a level of details sufficient to run accurate performance comparisons, it is virtually impossible to assess the performance of our proposed method against the “real-world” state-of-the-art.

In contrast, we hasten to say here that our method is based uniquely on received signal level measurements from known BSs/WiFi-Hotspots. These measurements are collected by default by standard user devices since each device continuously measures the received signal strength from BS beacon signals, in order to select the best cell and trigger handovers. Furthermore, these measurements are very robust since BS beacon signals are easy to detect and do not require any calibration or accurate timing and frequency synchronization, since they are simply wideband power measurements.

G. Our Contribution

Our contribution can be summarized as follows.

- We propose an accurate and computationally efficient localization method, merely based on RSS measurements, which does not necessitate additional signal processing or hardware (e.g., calibrated antenna arrays) at the user devices.
- Using the recently developed RadioUNet, one can estimate radio maps very efficiently and accurately, by using the knowledge of the propagation environment, e.g., a map of the city. Hence, we adopted it as a building block of the presented work, in order to achieve fast localization.
- The presented method relies on radio map (pathloss function) estimations and the measured received signal strength (RSS) values of anchor BSs at the UE of interest. Given the transmit powers of the BSs, one can compute the pathloss experienced by the UE from each BS. Based on these information and additional optional input features, the proposed neural network yields very accurate localization results, which are demonstrated by numerical experiments. The proposed method achieves about 5m of accuracy in mean absolute error, when trustworthy radio map estimates are available, which outperforms current state-of-the-art. Moreover, the method demonstrates high robustness to the inaccuracies in the radio map estimates in the realistic setting, while the compared RSS fingerprint-based methods' performances deteriorate greatly. We also provide extensive numerical comparisons with ToA ranging-based methods, where our method outperforms the state-of-the-art in different settings.
- The proposed method allows for localization at the UE side, which can find utility in, e.g., autonomous driving [46].
- We justify our neural network design by a comprehensive ablation study.
- We introduce two synthetic datasets which are publicly available for the research community.

The rest of the paper is organized as follows. We present the preliminaries in Section II. The proposed method is explained in Section III. Numerical results are presented in Section IV, and conclusions are drawn in Section V.

II. PRELIMINARIES

In this section, we present the preliminaries that serve as the building blocks of the proposed method.

A. Pathloss and Radio Map

Pathloss (or *large-scale fading coefficient*), quantifies the loss of wireless signal strength between a transmitter (Tx) and receiver (Rx) due to large scale effects. The signal strength attenuation can be caused by many factors, such as free-space propagation loss, penetration, reflection and diffraction losses by obstacles like buildings and cars in the environment. In dB scale¹, pathloss amounts to $P_L = (P_{Rx})_{dB} - (P_{Tx})_{dB}$, where P_{Tx} and P_{Rx} denote the transmitted and received locally averaged power (RSS) at the Tx and Rx locations, respectively. Notice that “locally averaged” power is defined as the energy per unit time averaged over time intervals of the order of a typical transmission slot in the underlying protocol (e.g., the duration of a Resource Block in 5G NR standard [47]) and over the whole system bandwidth. Hence, the effect of the small-scale frequency selective fading is averaged out and only the frequency-flat pathloss matters.

A *radio map* function $R(\mathbf{x}_1, \mathbf{x}_2)$ defines the pathloss between any two points \mathbf{x}_1 and \mathbf{x}_2 in the plane. For fixed Tx position $\mathbf{x}_1 = \mathbf{x}_{tx}$, the radio map is a function of the Rx position $\mathbf{x}_2 = \mathbf{x}_{rx}$, i.e., it can be represented as a 2-dimensional image where the value of the pathloss $R(\mathbf{x}_{tx}, \mathbf{x}_{rx})$ at each suitably discretized position \mathbf{x}_{rx} corresponds to a “pixel” of the image.

B. Radio Map Simulations

One well-known class of numerical methods for solving Maxwell’s equations in far-field propagation conditions is *Ray Tracing* [30]. In ray tracing, the signal is modeled as rays that are cast from the transmitter, travel in straight lines in homogeneous medium (like free space), and undergo rules of reflection, refraction and diffraction when the medium changes (e.g., when hitting an obstacle).

There are two main approaches for finding the ray paths in a given environment. Classical ray tracing searches for the paths between the transmitter and each receiver point, which necessitates very high computational time, with exponential dependency between the number of interactions and the complexity of the geometry (e.g., the number of buildings), and a linear dependency between the computation time and the number of receiver pixels [48]. The second approach, ray launching [49], discretizes the propagation angle at the transmitter and launches rays in all directions. The rays interact with the environment as before, and terminate when a predetermined

¹ $(\cdot)_{dB} := 10 \log_{10}(\cdot)$.

maximum number of interactions is reached or when the signal strength goes below a minimum value. The received signal strength is then computed as the sum of all rays at all receiver pixels (i.e., discretized locations).

In the following, we briefly explain the simulation models used in this paper, computed using the software WinProp [31].

1) *Dominant Path Model (DPM)* [50]: DPM is based on the assumption that the dominant propagation path from Tx to Rx must arrive via convex corners of the obstacles to Rx, and thus only diffractions are taken into account, omitting reflections and penetrations altogether. The model assigns the pathloss of the ray with the largest received power to each receiver point. This is equivalent to finding the shortest free space path to each point, and computing the corresponding pathloss.

The formula of the pathloss is given by some statistical model, based on the following parameters as inputs: The length of the path, a parameter that depends on the distance and visibility between the Tx and Rx, and a diffraction loss function, which depends on the angle of the diffraction and the number of previous diffractions in the path. The model can also consider waveguiding pathloss effects when calculating the pathlosses of the paths, where reflection loss of the walls along the path as well as their distance to the path influence the value. This simplified model of the signal propagation allows a very efficient implementation with respect to more traditional ray tracing methods.

2) *Intelligent Ray Tracing (IRT)* [48]: This algorithm starts with a pre-processing step for the considered map, where the faces of the obstacles are discretized into regular tiles, their edges into segments, and the visibility relations among the centers of these elements are found. For the visible element pairs, the distance between the centers of them and the subtended angles are calculated. The computations of the paths, based on the ray launching approach, are then accelerated using the pre-computed visibility model. The maximum number of interactions is set by the user.

In our simulations, we set the maximum number of interactions as two (at most two diffractions or two reflections). We set the tile length as 100 m, which results in having only one tile for most of the building walls and for all of the cars (cf. Section III-B for the detailed description of the dataset).

C. RadioUNet

RadioUNet is a UNet-based [51] pathloss radio map estimation method introduced in [40], [52]. In this paper we use the so called RadioUNet_C, which is a function that receives the map of the city and the location of a BS and returns an estimation of the corresponding radio map with a high accuracy, with root-mean-square-error of order of 1dB in various scenarios, and a run-time order of milliseconds on NVIDIA Quadro GP100 [40]. RadioUNet is trained in supervised learning to match simulations of radio maps, using the RadioMapSeer Dataset [53].

III. PATHLOSS FINGERPRINT-BASED LOCALIZATION WITH DEEP LEARNING

In this section we present LocUNet – a deep learning localization method based on estimations of pathloss radio maps.

A. Proposed Method

Suppose that a user with location $\mathbf{x}_U = (x_U, y_U)$ reports the strength of beacon signals (Non-interfering identification signals), transmitted from a set of BSs B_j , $j = 1, \dots, J$, with known coordinates $\mathbf{x}_{B_j} = (x_{B_j}, y_{B_j})$. Based on the relation between transmit/receive powers and the pathloss $(P_{\text{Rx}})_{\text{dB}} = P_{\text{L}} + (P_{\text{Tx}})_{\text{dB}}$, the pathloss between the device and the BSs, p_j , $j = 1, \dots, J$, can be calculated, where we assume the small-scale fading effects are eliminated by averaging over time and system bandwidth. In our approach, the position of the UE is estimated based on the following information.

- 1) The pathloss values p_j , $j = 1, \dots, J$,
- 2) The estimations of the radio maps for each BS $R_j(x, y) := R(\mathbf{x}_{B_j}, (x, y))$, $j = 1, \dots, J$, computed via RadioUNet,²
- 3) The map of the urban environment, the locations of the BSs (which are fixed and known).

The processing is typically performed by centralized processing in the cloud, based on the RSS information reported by the UE. Alternatively, localized processing at the UE may also be considered, but in this case the UE must be aware of the BSs location (beyond their identity) and of the corresponding radio maps. At this point we do not distinguish between these two options, which are equivalent in terms of system performance (although may not be equivalent in terms

²From now on it is convenient to represent the locations as pixel coordinates (x, y) in the 2-dimensional plane.

of protocol overhead, computation complexity at the UE, and privacy of the UE location with respect to the network control).

Our method, called LocUNet, computes an estimation of the location of UE using a UNet variant. In order to input the above information (1)–(3) to the UNet, they are first represented as a set of 2D images.

- 1) The RSS values $\{p_j\}$ are converted to gray-level. Each pathloss p_j is represented as a 2D image $P_j(x, y)$ of a constant value p_j , i.e., for each j this is an all-gray uniform image, but the level of gray differs for different indices j .
- 2) Each radio map $R_j(x, y)$ is represented as a 2D image, with pixel values in gray-level. Radio maps are obtained by using RadioUNet, which takes the map of the urban environment, and the locations of BSs as input features [40].
- 3) The map of the urban environment is represented as a binary black and white image, where the interior of the buildings are white (pixel value = 255), and the exterior is black (pixel value = 0).
- 4) The location of each BS B_j is represented as a one-hot binary image, where the pixel at location (x_{B_j}, y_{B_j}) is white, and the rest is black.

Inputs (3) and (4) are optional for LocUNet (Note that they are still needed to generate the input (2) via RadioUNet), and through numerical experiments we observe their negligible influence on the performance (See Section IV-F1).

The first part of LocUNet is a UNet [51], with average pooling, upsampling + bilinear interpolation, and Leaky ReLU (with parameter 0.2) as the activation function. We call the output feature map of the UNet, $H(x, y)$ a *quasi-heatmap*, as its value at a point (x, y) in the map quantifies the likelihood of the UE to be located at this point, while it can take negative values, due to LeakyReLU being the activation function of the network.

The final layer of LocUNet computes the center of mass (CoM) (μ_x, μ_y) of the quasi-heatmap $H(x, y)$,

$$\mu_x = \frac{\sum_{x=1}^{256} \sum_{y=1}^{256} xH(x, y)}{\sum_{x=1}^{256} \sum_{y=1}^{256} H(x, y)}, \quad \mu_y = \frac{\sum_{x=1}^{256} \sum_{y=1}^{256} yH(x, y)}{\sum_{x=1}^{256} \sum_{y=1}^{256} H(x, y)},$$

where 256 is the number of pixels along each axis. Note that the CoM calculation admits a convolutional representation as well, rendering the LocUNet a fully-convolutional neural network as whole.

LocUNet										
Layer	In	1	2	3	4	5	6	7	8	9
Resolution	256	256	128	64	64	32	32	16	16	16
Channel	<i>in</i>	20	50	60	70	90	100	120	120	135
Filter size	3	5	5	5	5	5	5	3	5	5
Layer	10	11	12	13	14	15	16	17	18	19
Resolution	8	8	4	4	2	4	4	8	8	16
Channel	150	225	300	400	500	400 + 400	300 + 300	225 + 225	150 + 150	135 + 135
Filter size	5	5	5	5	4	5	4	5	4	5
Layer	20	21	22	23	24	25	26	27	28	29
Resolution	16	16	32	32	64	64	128	256	256	256
Channel	120 + 120	120 + 120	100 + 100	90 + 90	70 + 70	60 + 60	50 + 50	20 + 20 + <i>in</i>	20 + <i>in</i>	1
Filter size	3	6	5	6	5	6	6	5	5	-

TABLE I: Architecture of the first part of LocUNet (w/o final CoM layer). *Resolution* is the number of pixels of the image in each feature channel along the x, y axis. *Filter size* is the number of pixels of each filter kernel along the x, y axis. The input layer is concatenated in the last two layers before the CoM layer. $in = 10/11/15/16$, cf. Table VIII.

The architecture of LocUNet is summarized in Table I.

We measure the accuracy of the proposed method with average Euclidean distance (AED) between the estimated UE location and the ground-truth location. Namely, with

$$L_{\text{AED}}(\mathbf{u}, \tilde{\mathbf{u}}) = \frac{1}{|\mathcal{S}|} \sum_{k \in \mathcal{S}} \|\mathbf{u}^k - \tilde{\mathbf{u}}^k\|_2, \quad (1)$$

where $\tilde{\mathbf{u}}^k := (\mu_x^k, \mu_y^k)$ and $\mathbf{u}^k := (x_U^k, y_U^k)$ denote the LocUNet estimation and the ground-truth of the k th instance of the dataset, and \mathcal{S} is the entire training set.

We also consider using the average squared Euclidean distance (ASED) as a loss function, which is the average squared 2D Euclidean distance

$$L_{\text{ASED}}(\mathbf{u}, \tilde{\mathbf{u}}) = \frac{1}{|\mathcal{S}|} \sum_{k \in \mathcal{S}} \|\mathbf{u}^k - \tilde{\mathbf{u}}^k\|_2^2. \quad (2)$$

When using stochastic gradient descent for training, we take $\mathcal{S} = \mathcal{B}_m$ in one of the losses mentioned above, where \mathcal{B}_m is the m th mini-batch of the training set.

B. Datasets

We introduce two new datasets to allow for comparisons among RSS (pathloss) and ToA ranging-based algorithms. These two new datasets, which we call *RadioLocSeer Dataset* and *RadioToASeer Dataset*, can be found at <https://RadioMapSeer.GitHub.io/LocUNet.html>.

1) *RadioLocSeer Dataset*: We introduce a dataset of city maps, BS locations, and the corresponding radio maps simulated by the ray-tracing software WinProp [31] and by RadioUNet. The dataset is based on the test set of RadioMapSeer [40], which contains 99 maps and 80 BS

Parameter	Value
Map size	256^2 pixels
Pixel length	1 meter
Tx, Rx height	1.5 meter
Center carrier frequency	5.9 GHz
Channel bandwidth	10 MHz
Noise power spectral density	-174 dBm/Hz
Transmit power	23 dBm
Noise floor	-134 dB

TABLE II: RadioLocSeer Dataset parameters.

per map. We report the parameters of the dataset in Table II (cf. [40] Section III.B for details). The maps are randomly split into 69 training, 15 validation and 15 test maps.

For each map we randomly generate 200 UE positions and randomly pick 5 BS positions out of the 80 available ones. We repeat the latter step 50 times for each map, to represent different scenarios of BS deployment. The BS locations are chosen to be separated by at least 20m. Moreover, the BSs and UEs are restricted to lie in the middle 150×150 and 164×164 boxes about the center of the 256×256 grid of the RadioMapSeer images, respectively.

For each of the above maps and BS location, we provide DPM radio map estimations via RadioUNet (see Subsection IV-A), in addition to the simulated (by WinProp) radio maps of the propagation models, DPM and IRT (cf. Sec. II-B). For IRT simulations, we provide a second version which includes the effects of cars as additional obstructions, where each map consists of 100 cars (if the roads of the corresponding maps are of sufficient length to fit them, otherwise the maximum number that can fit) of size $2 \times 5 \times 1.5$ (width \times length \times height), randomly generated near and along or perpendicular to roads. We also provide the images of the city maps, along with the coordinates of the considered BSs and the UEs.

2) *RadioToASeer Dataset:* We generated another new dataset based on the dominant path model (cf. Subsection II-B1) via the software *WinProp* [31], of the same settings as in RadioLocSeer Dataset, which provides ToA information of the dominant paths, to allow for comparisons between RSS and ToA ranging-based methods in realistic urban scenarios.

We argue that using this dataset serves as quasi-lower bounds for the errors of the ToA ranging-based methods, as explained next.

Remark 3: We call the straight line connecting Tx and Rx, which may go through obstacles (in this paper, buildings and cars), the direct path. The difference (error) between ranging with ToA measurement of the ray (range is calculated as: $ToA \times \text{the speed of light}$) and the direct

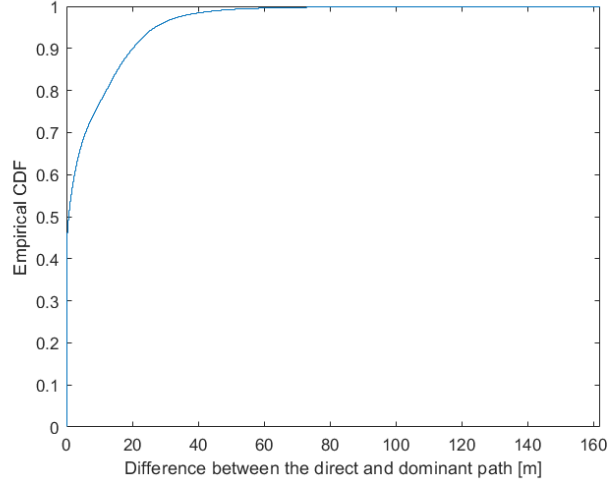


Fig. 1: Empirical CDF of the difference between the direct and dominant path in meters

path is called the NLOS bias, which is by definition non-negative (Zero when the link is in LOS, positive otherwise). The empirical cumulative distribution function (CDF) of the NLOS bias of the dataset is shown in Fig. 1. We observe that 47% of the links in the RadioToASeer Dataset are in LOS.

We argue that even though the dominant path is a NLOS path in general, and hence introduces an NLOS bias, it is quasi-optimal to use the ToA of such paths in ToA ranging-based algorithms.

First of all, the NLOS bias of a dominant path is lower than that of a potential free space path between the same Tx and Rx, that undergoes reflections to reach its destination (cf. Section II-B1). Thus, relying on ToAs of the dominant paths would yield better performances than the ToAs of the other free space paths.

As a matter of course, using the length (range) of the direct path would be optimal. However, the signal corresponding to the direct path is highly unlikely to be detected, as explained next.

First, we note that empirical evidence shows that loss due to penetration through a building is around 15 – 20dB [54]. In an urban scenario, the associated direct path of an NLOS link is usually subject to blockage by numerous buildings. For devices with realistic noise figures and SNR requirements, the received power of such a path may go easily below the detection threshold.

Moreover, the bandwidth considered in the current paper does not allow for a well resolvability of the multi-path components. Indeed, in the considered setting, we have $\Delta\tau = 1/W = 100\text{ns}$, so, when multiplied with the speed of light $c \approx 3 \times 10^8 \text{ m/s}$, the difference between the paths

should be at least $\Delta d = c\Delta\tau = 30\text{m}$ for resolvability. In our dataset, we observe that around 92% of NLOS direct paths don't satisfy this condition (cf. Fig 1), i.e., the difference of the length of the direct path and that of the dominant ray is less than 30m.

Lastly, whenever the direct path penetrates an obstacle, there is the so-called excess delay

$$t_{\Delta} = (\sqrt{\epsilon_r} - 1) \frac{d_w}{c}. \quad (3)$$

Here, t_{Δ} is the excess delay, ϵ_r denotes relative electric permittivity, and d_w stands for the thickness of the wall. Assuming a total length of 3m of penetrated wall of concrete with permittivity 4, we get an excess delay of 10ns, which further makes the ToA of the direct and dominant path closer, deteriorating resolvability further: about 94% of NLOS direct paths don't satisfy this.

Hence, it is reasonable to ignore the direct paths and use the dominant paths instead.

Moreover, the dataset assumes exact ToA information, i.e., perfectly synchronized clocks at the BSs and UEs, and also no other additive noise on ToA measurements.

Thus, all in all, evaluating the ToA ranging based-methods on this dataset yields quasi-upper bounds for their performances.

C. Training

We perform supervised learning on the training set. We use Adam optimizer [55] with an initial learning rate of 10^{-5} and decrease the learning rate by 10 after 30 epochs. We set the total number of epochs for training as 50 and batch size as 15. To avoid overfitting, we pick the network parameters with the lowest validation error in the 50 training epochs. We used PyTorch [56] for the implementation³.

Remark 4: To the best of our knowledge, there exists no publicly-available dataset of measured radio maps that represent the signal strength or ToA with a fine resolution, which is crucial for the localization task. As mentioned before, establishing real radio maps requires very expensive site surveying efforts, which is beyond the means of academic institutions. We note that many previous works in communications relied on synthetically generated ground-truths. Some works that used ray-tracing are [15], [26], [32]–[39], [57]–[63]. Other recent works that relied on computationally generated ground-truths are [64]–[71], to name a few.

³The code is available at <https://GitHub.com/CagkanYapar/LocUNet>. For reproducibility, see the compute capsule at <https://codeocean.com/capsule/7149386/tree>.

Moreover, one of the main arguments of the current work is the “inevitability” of the mismatches between the radio map estimations and the true (real-life) radio maps. Hence, for the localization problem at hand, modelling the mismatches turns out to be “the goal”, which we can decouple from the availability of real-life measurements. We explain this later in detail (Remark 6).

IV. NUMERICAL RESULTS

In this Section, we demonstrate the performance of LocUNet by numerical simulations. We assess the accuracy of LocUNet and the compared methods on the test set, namely, by AED (1) with $\mathcal{S} = \mathcal{T}$, where \mathcal{T} is the test set (cf. Subsection III-A).

First, we describe two settings in order to investigate the robustness of our method to realistic inaccuracies in the input radio map estimates with respect to the true radio maps. Afterward, we illustrate these scenarios and LocUNet’s estimation results under them by picking two instances (one generic and one critical) from the test set of the RadioLocSeer Dataset. Then, we compare the performance of the presented method with state-of-the-art fingerprint-based and ToA ranging-based methods. The conducted numerical experiments show that LocUNet outperforms all the previously state-of-the-art methods in numerous settings. Next, we present the baseline/relevant previous methods, discuss their relation with LocUNet, and present their numerical evaluations. Finally, we present the “ablation study” of input features, activation function of the layer before the CoM layer, and the loss function for training, which justifies our choices.

All of the compared algorithms with CPU implementation were run on an Intel Core i7-8750H, and LocUNet was run on a GPU of NVIDIA Quadro RTX 6000. We report the approximate run-times of the LocUNet and the compared algorithms (all implemented using MATLAB, run on CPU), as well. We note that none of our implementations were meant to optimize the run-time, and hence the reported times don’t reflect a fair assessment.

Remark 5: *The numerical results in the following are obtained with the above mentioned high computational power, which cannot be available at a usual UE. Hence, they showcase the localization performance of the LocUNet when run at a central unit (e.g. in the cloud), based on the reported RSS values of the UE for each BS. We hope that adapting the RadioUNet (which we use in order to obtain fast and accurate radio map estimations) and the proposed LocUNet to the hardware limitations of a UE (so that the proposed method can be performed locally), e.g. by knowledge distillation [72], won’t degrade the overall performance remarkably. The*

investigation of this problem is however outside the scope of the current paper and is left as future work.

A. Robustness Analysis

As we argued before (cf. Section II-A), the RSS values are obtained by integrating the signal strength measurements over time and the channel bandwidth, which effectively averages out the small scale frequency selective fluctuations.

Given this, we identify three sources of mismatch between the true (real) RSS (pathloss) radio maps (i.e., where the measurements at the UE stem from, or in other words, the radio map which is established by true measurements) and the estimated ones, which are used as input features of LocUNet.

- 1) The mismatch between the real propagation phenomena (governed by Maxwell's equations) and the simplified model which is used to estimate the radio maps. Here, a statistical model based on radial symmetry exemplify a very simplified model with great mismatch, whereas models that use the geometry of the environment (e.g. ray-tracing methods or their accurate approximations like RadioUNet) will yield much better radio map estimations. Such methods, obviously, suffer from
- 2) The mismatch due to the inaccurate knowledge of the propagation environment. Here, the inaccuracies occur due to two reasons: **1)** Inaccuracies of the position and shape information of the objects which are stationary, **2)** Mobility of the objects. For stationary objects in the environment, a good description of the shapes of stationary objects (e.g. buildings) can be obtained with some feasible effort (Maps of many cities are available for public access, e.g. by *OpenStreetMap* [73], and further refinements of the stationary environment could be attained by for instance computer vision techniques, based on e.g. street level or satellite images of the environment, or by methods which use LiDAR). However, it is very difficult to alleviate the inaccuracies due to the mobility of the objects, as: **a)** Estimating the shape of an object is a very demanding task, which is impossible to apply for every moving object in the environment. **b)** Even if it was possible to know their shapes (e.g., for cars, their shape could be fetched from a database), their accurate position would not be available due to their mobility.

Hence, in the following we focus on the inaccuracy due to mobile objects, which we modeled as the presence of cars in the environment, unknown to LocUNet while estimating

the radio maps.

- 3) A milder mismatch occurs due to the speeding up of the radio map computations, which in the current paper is as a result of using RadioUNet as the radio map estimator, instead of a ray-tracing software.

To study the performance of LocUNet under first source of mismatch described above, we take the dominant path model (DPM, cf. Sec. II-B1) as the model for the radio map estimations, and the intelligent ray-tracing (IRT, cf. Sec. II-B2) as the *surrogate for the real* propagation phenomena, from which the UE gets its measurements. We justify this approach in the following Remark.

Remark 6: *Our rationale for this decision is as follows: Both the DPM and IRT are proven to yield good approximations of real radio maps, while differing from each other to a considerable extent in how they calculate the pathloss: DPM is purely based on the dominant paths, excluding the reflected rays altogether, whereas IRT computations are in general dominated by the reflected rays. Putting emphases on different partial phenomena of the real propagation physics, it is reasonable to assume that their estimations differ approximately as much as DPM (or IRT, our choice of DPM being the estimation model and IRT being the surrogate for real-life/ground-truth⁴ is arbitrary) differs from the real radio maps. Hence, we argue that our numerical results serve as a good representative of the performance of LocUNet, when it is trained by using real-life pathloss measurement datasets.*

In the following we designate two scenarios with increasing compliance with the reality, encompassing the above mentioned sources of inaccuracies.

1) *Nominal Scenario:* In this very optimistic scenario, we assume that the real radio maps are *exactly* governed by DPM and the radio map estimates are obtained by RadioUNet, which was trained in supervised fashion to estimate radio maps under DPM assumption, as well. Moreover, we assume that there are *no additional unknown obstacles*, i.e., the *exact* information about the propagation environment is available to RadioUNet. Hence, LocUNet enjoys having access to very high accuracy radio maps, where the inaccuracy of the available radio maps with respect to the true radio maps is solely due to the prediction error of RadioUNet, addressing the third above mentioned source of inaccuracy.

⁴Throughout the paper, we use the terms “real-surrogate” and “ground-truth” interchangeably.

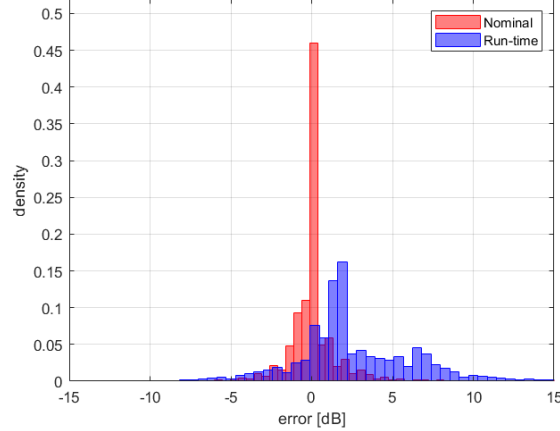


Fig. 2: Histograms of the differences between the estimated (by RadioUNet, which was trained to estimate the DPM simulations) and the assumed ground-truth pathloss measurements in RadioLocSeer Dataset. The Nominal and Robustness Scenarios use radio maps generated by DPM simulations, and IRT simulations with additional obstructions (cars) in the propagation environment, as surrogate ground-truths, respectively.

2) *Robustness Scenario:* This scenario encompasses all the inaccuracies enumerated previously, which are inevitable in the real deployment of the method. That is to say, we take into account the mismatch between the real radio maps (above mentioned first source of error), which we simulate by IRT as a real-surrogate, and the estimated radio maps, which are obtained by RadioUNet that was trained on DPM dataset. We also add the effects of unknown obstructions to the real-surrogate IRT simulations, addressing the second above mentioned source of error. We model the obstructions as cars (100 per map in general, cf. Sec. III-B).

In RadioLocSeer Dataset, we provide the associated estimated (DPM predictions by RadioUNet [40]) and simulated (to serve as real-surrogate) radio maps (DPM, IRT, and IRT with cars simulations by WinProp [31]) for each scenario (cf. Section III-B1). The root mean square error between the estimated and the simulated real-surrogate pathloss measurements are found to be 1.66 dB and 4.80 dB, for the Nominal and the Robustness Scenarios, respectively. And the mean absolute errors for the respective scenarios are 0.87 dB and 3.55 dB. The histograms of the differences between the estimated and real-surrogate pathlosses are shown in Fig. 2 for each scenario.

3) *Robustness to Out-of-Distribution Pathloss Measurements:* In this Section we show the performance of LocUNet for the above defined two scenarios under out-of-distribution (OOD) pathloss measurements. To this end, we test the trained networks with pathloss measurements obtained from different simulations scenarios. In addition to the above mentioned two ground-

truth scenarios (DPM and IRT with cars), we consider two more scenarios. **1)** DPM with cars, where the radio map is simulated with the DPM under the presence of additional (unknown to LocUNet) obstructions (cars), **2)** IRT simulations as in the Robustness Scenario, but without the presence of unknown obstructions.

We observe that the network trained in the Nominal scenario suffers from substantial decrease of performance when the pathloss measurements stem from other scenarios, whereas the accuracy of the network trained in Robustness Scenario is not much affected. We also notice that the network trained in Robustness Scenario performs even better when there are no unknown cars in the map.

These results demonstrate that training LocUNet using radio map estimations that are different from the reality (Robustness Scenario), is in fact more robust to OOD pathloss measurements than the LocUNet trained with very good estimates of real-life radio maps (Nominal Scenario).

	DPM	DPM w/ cars	IRT	IRT w/ cars
Nominal	4.73	8.80	20.50	23.85
Robustness	13.63	13.12	11.84	12.85

TABLE III: Neural networks of the Nominal and Robustness Scenarios evaluated under out-of-distribution pathloss measurements. The accuracies under in-distribution measurements are shown in red.

B. Examples

In Figures 3 and 4, we show the results of LocUNet for two example test maps in the previously explained Nominal and Robustness scenarios, where Fig. 3 and Fig. 4 are examples of critical (very low RSS/high pathloss at the UE for each BS beacon) and typical UE reception scenarios in RadioLocSeer Dataset.

In each of the figures, in the first two rows, we show the simulated radio maps for the considered 5 BS locations, which serve as the real-surrogate (ground-truth) (From top to bottom): DPM ground-truth (for the pathloss measurements at UE in the Nominal Scenario), IRT with cars ground-truth (for the Robustness Scenario). In the third row, the DPM estimations via RadioUNet are shown.

In the last rows, we show the heatmaps and the locations estimations (i.e., the CoM of the quasi-heatmap, marked with yellow squares) of the LocUNet for the considered three scenarios, where we partitioned the quasi-heatmap in two partial heatmaps, representing the positive and

the negative values (normalized by its max. and min. pixel value, respectively), which we call the *positive heatmap* and the *negative heatmap*. The true location of the UE is marked with green cross.

In each scenario, we observe that one of the heatmaps (the positive ones for the first scenario, and the negative one for the second scenario⁵) serves as a *belief map* about the location of the UE, while the other one as a *disbelief map*. We see that the non-zero pixels (There are much more of them in the Nominal Scenario) of the disbelief maps are concentrated on the pixels occupied by the buildings and are distanced from the neighborhood of the estimated location.

Another observation we make, is that, with increasing mismatch (i.e. from the first to the last scenario) between the radio map estimations and the real-surrogate simulations, the number of pixels occupied by the disbelief map reduces. This demonstrates the diminishing confidence of the LocUNet about where the UE is *not* located at, while the uncertainty due to propagation model and the environment knowledge mismatch increases.

In all the scenarios, the city maps and the Tx locations were given as additional inputs to LocUNet.

C. Comparison with Pathloss Fingerprint-Based Methods

In Table IV, we present the AED accuracy of LocUNet in the scenarios described in Subsection IV-A, and compare its performance with the competing fingerprint-based methods. The data is provided by the RadioLocSeer Dataset III-B1. In order to study effect of number of BSs on the performance, we also pick a random subset of 3 BS the 5 BS provided by the dataset for each map and BS deployment and evaluate our method there. We compare with two fingerprint-based methods, namely, *k-nearest neighbors (kNN)* method [74] and an adaptive kNN variant [75]. We determined the k parameters of the kNN algorithm by coarse grid-search for both of the 3 and 5 BS settings.

We observe that LocUNet provides the best accuracy among the fingerprint based methods in all the scenarios, and LocUNet is especially good at dealing with the inaccuracies of the radio map estimations in the realistic setting, as witnessed in the results of the Robustness Scenario. Recall that the considered inaccuracies are unavoidable in a realistic urban setting (Sec. IV-A). Thus, the results in this scenario are a more meaningful indicator for the performances of the

⁵Notice that the CoM of the quasi-heatmap is invariant to the multiplication of the quasi-heatmap by -1 .

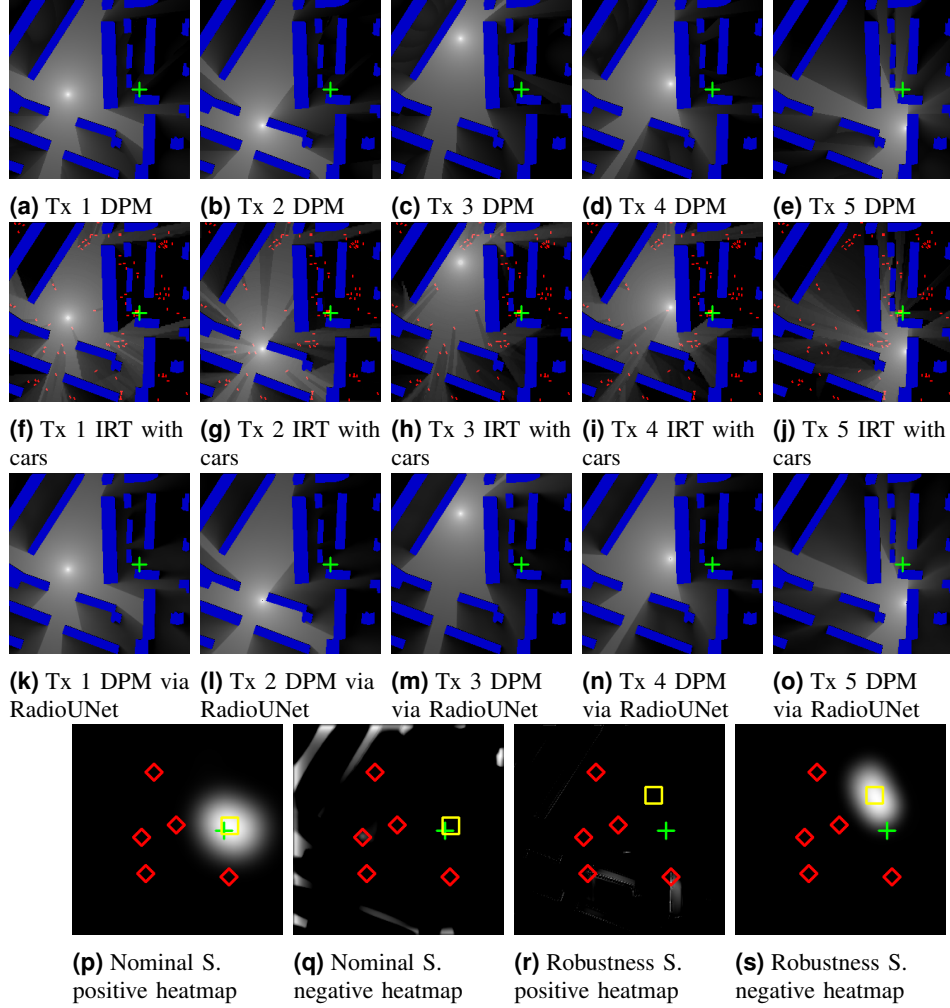


Fig. 3: A critical localization problem, where the pathloss at the UE from each BS is very high. **First row:** DPM true radio maps. **Second row:** IRT with cars true radio maps. Cars are shown in red. **Third row:** DPM estimated maps by RadioUNet. **Fourth row:** LocUNet results for the two scenarios. The normalized positive (by max. pixel value) and the negative (by min. pixel value) heatmaps of LocUNet before CoM layer are shown in gray-level. Buildings are blue, Tx locations are marked with red diamonds. Estimated and true locations are marked with yellow square and green cross, respectively.

compared algorithms. Here, LocUNet outperforms the best performing competitor algorithm (kNN) by about 14m and 19m in AED in the cases of 5 or 3 BSs per a city map.

Remark 7: We attribute the success of LocUNet in accuracy and its robustness to the inaccuracies in radio map estimations to its fully-convolutional nature, which takes into fully account the neighborhood/spatial relations in the radio map estimations, whereas the kNN method makes use of the spatial information only when the CoM of the k -nearest-neighbors are found in the final step. Note that both kNN and our method perform CoM as the last step and the found k -

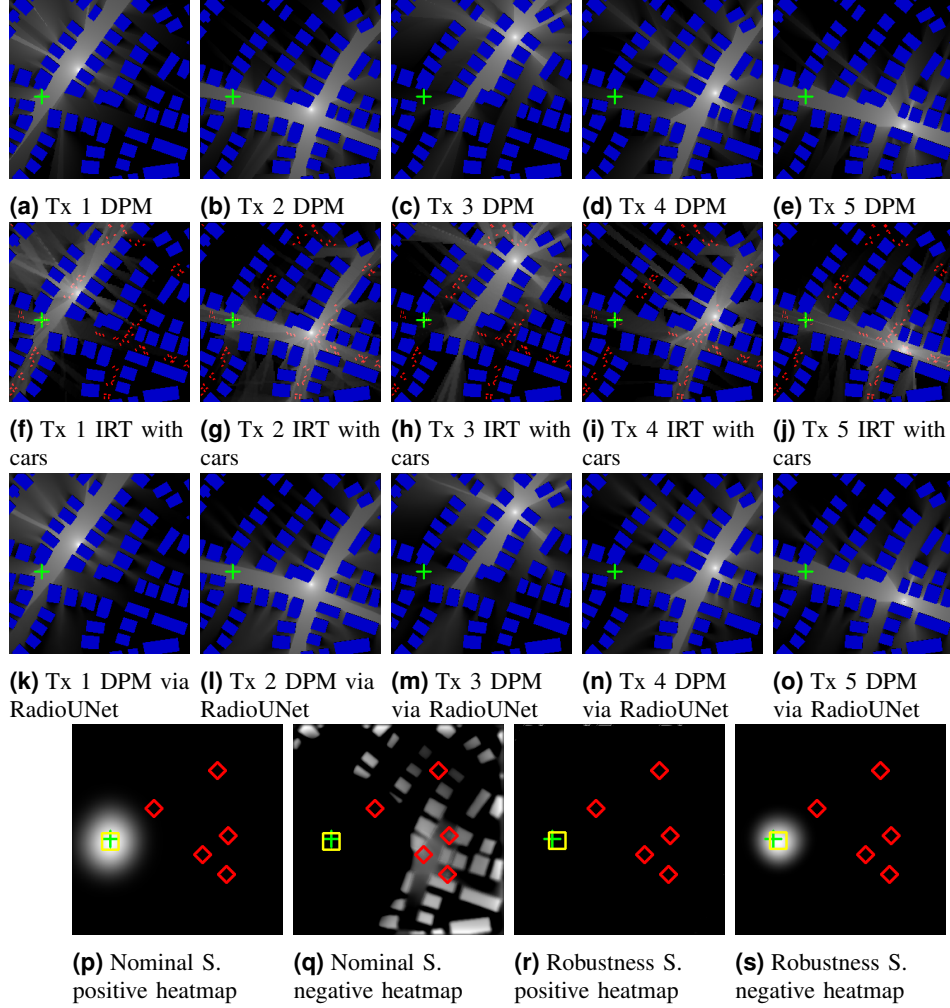


Fig. 4: A generic localization problem of our dataset, where the pathloss at the UE from each BS is moderate. **First row:** DPM true radio maps. **Second row:** IRT with cars true radio maps. Cars are shown in red. **Third row:** DPM estimated maps by RadioUNet. **Fourth row:** LocUNet results for the two scenarios. The normalized positive (by max. pixel value) and the negative (by min. pixel value) heatmaps of LocUNet before CoM layer are shown in gray-level. Buildings are blue, Tx locations are marked with red diamonds. Estimated and true locations are marked with yellow square and green cross, respectively.

nearest-neighbors can be interpreted as a heatmap. However, the k -nearest-neighbors are solely determined by assigning each pixel a distance in the signal space of the RSS values under a metric (we took the usual “Euclidean”, the square root of the sum of the squared residuals), which disregards any spatial relations of the pixels.

Our method, in contrast, benefits from the neighborhood relations of the pixels thanks to its fully-convolutional nature, and the prior information from the estimated radio maps are much more effectively utilized.

Algorithm	5Tx	3Tx	ms
Nominal Scenario			
kNN [74] (k=16, 40)	7.01	17.27	~ 20
Adaptive kNN [75] (avg. k=2.50, 2.40)	7.49	16.18	~ 20
Proposed LocUNet	4.73	10.19	~ 5
Robustness Scenario			
kNN [74] (k=300,1500)	27.19	38.54	~ 20
Adaptive kNN [75] (avg. k=8.51, 5.08)	29.51	45.31	~ 20
Proposed LocUNet	12.85	19.28	~ 5

TABLE IV: Comparison with fingerprint-based methods. Average Euclidean distance (AED) for 5 and 3 number of BSs, and approximate run-times of the evaluated methods.

1) *Conditional Performance of the Compared Methods:* Previously, we have evaluated LocUNet and the kNN algorithms for 5 BS deployments or for random subsets of 3 BS deployments of them. In the following, we report the performances of LocUNet and kNN, conditioned on the number of BSs with beacon signals above the noise floor (detectable at the UE), and above 10dB of the noise floor. Notice that 0 (black) pixels of the radio maps are in fact the points below or at the noise floor (cf. [40] Section III.B for details).

In Table V we demonstrate the conditional performance of LocUNet and kNN in the Robustness Scenario, conditioned on the number of detectable BSs with received signal strengths of beacon signals being above the noise floor, and above 10dBs of the noise floor. We observe that LocUNet deals much better with low number of detectable BSs and with low received powers than the kNN.

No BS above NF	0	1	2	3	4	5	Overall
kNN	98.80	66.55	47.75	34.32	26.31	19.62	27.19
LocUNet	27.32	30.72	22.51	16.31	12.88	9.09	12.85
no instances in test set	34(0.02%)	3330(2.2%)	12484(8.3%)	26527(17.7%)	35121(23.4%)	72504(48.3%)	150000
No BS above 10dB of NF	0	1	2	3	4	5	Overall
kNN	83.63	55.96	36.49	25.26	20.93	17.80	27.19
LocUNet	34.92	26.70	17.41	12.71	10.11	7.65	12.85
no instances in test set	1665(1.1%)	12270(8.2%)	25192(16.8%)	34033(22.7%)	33793(22.5%)	43047(28.7%)	150000

TABLE V: Conditional performances of kNN ($k = 300$) and LocUNet.

D. Comparison with ToA Ranging-Based Methods

Using the RadioToASeer Dataset (Sec. III-B2), we evaluate the accuracies of the state-of-the-art ToA ranging based algorithms, in our presented realistic urban setting, and compare with our method. The compared methods are based on the measured ToAs (of the dominant paths) of the

beacon signals of BSs. In the following, we present the numerical results for the case of noise-free ToA measurements and for the more realistic noisy ToA measurements case. Recall that (cf. Remark 3), using the RadioToASeer Dataset for these methods yields quasi-upper bounds for the performances of these algorithms for real-life ToA measurements, due to the optimistic assumption of resolvable dominant paths, which are more likely to be detected than the direct paths.

1) *Noiseless ToA measurements:* For the compared algorithms, we set the noise standard deviation parameter as $\sigma = 0.0001$ meter for the relevant methods. For the robust ToA methods [20]–[22], we pick the NLOS bias b at CDF 0.9 (20m), as suggested in [23], and also at CDF 0.5 (0.7m) (cf. Fig. 1) (cf. Remark 3 for the discussion on the dataset).

We report the simulation results in Table VI. For a reasonable comparison in terms of fairness, we compare the performance of these methods with the LocUNet in the Nominal Scenario (cf. Subsection IV-A1), which is also shown.

Notice that both the ToA ranging-based methods and LocUNet are evaluated in the DPM setting, but the ToA methods use the exact length of the dominant path, whereas the pathloss values available to LocUNet are not only determined by the path length, but also by additional interaction losses due to the diffractions at the corners of the obstacles. Hence, the ToA methods have access to more informative/less ambiguous location information through measurements than LocUNet.

We observe that in these very optimistic scenarios for both LocUNet and ToA ranging-based methods, AEDs of LocUNet are 4.73m (5 BS per map) and 10.19m (3 BS per map), where the best result among ToA ranging-based methods are 7.16m (5 BS per map) and 10.85m (5 BS per map).

2) *Noisy ToA measurements:* We report in Table VII the numerical evaluations of the ToA ranging-based methods under a more realistic scenario, where prominent sources of ToA measurement errors are taken into account. The performance of the realistic Robustness Scenario of LocUNet is also shown for comparison. We considered 3 BSs per map, for all the methods.

There are several factors which deteriorate the accuracy of ToA measurements at a UE, e.g. clock offset and skew (synchronization errors), quantization of the measured values, additional thermal noise, or failures in resolving the multipath components. In the numerical experiments, we only took into account the inaccuracy due to the quantization (in LTE, ToAs are quantized to intervals of 9.77 meters), the thermal noise and the clock error and modeled them altogether

Algorithm	5Tx	3Tx	ms
POCS [17], [18]	37.89	46.28	~ 15
SDP [19]	7.16	12.92	~ 600
Robust SDP 1 [20], $b = 20$	10.14	13.23	~ 600
Robust SDP 1 [20], $b = 0.7$	7.55	10.85	~ 600
Robust SDP 2 [21], $b = 20$	12.29	18.68	~ 600
Robust SDP 2 [21], $b = 0.7$	7.63	14.66	~ 600
Bisection-based robust method [22], $b = 20$	10.11	15.94	~ 16
Bisection-based robust method [22], $b = 0.7$	9.49	15.01	~ 16
Max. correntropy criterion method [23]	12.45	18.47	~ 30
LocUNet Nominal Scenario	4.73	10.19	~ 5

TABLE VI: Comparison with ToA ranging-based methods. Absolute Euclidean distance accuracies and approximate run-times of compared algorithms are shown. $\sigma = 0.0001\text{m}$ for ToA ranging-based algorithms. Results for 3 and 5 anchor BSs.

Algorithm	$\sigma = 10$	$\sigma = 20$
POCS [17], [18]	47.37	48.82
SDP [19]	24.76	39.43
Robust SDP 1 [20], $b = 20$	23.95	36.56
Robust SDP 1 [20], $b = 0.7$	26.04	39.17
Robust SDP 2 [21], $b = 20$	26.96	37.81
Robust SDP 2 [21], $b = 0.7$	26.44	39.16
Bisection-based robust method [22], $b = 20$	25.37	38.18
Bisection-based robust method [22], $b = 0.7$	27.29	40.92
Max. correntropy criterion method [23]	31.25	45.72
LocUNet Robustness Scenario	19.28	

TABLE VII: Comparison with ToA ranging-based methods subject to additive ToA measurement noise. Absolute Euclidean distance accuracies and approximate run-times of compared algorithms are shown. $\sigma = 10, 20$ meters for ToA ranging-based algorithms. The number of anchor BSs is 3.

with a single additional Gaussian noise variable with zero mean and standard deviation σ , as proposed in [76]. As in [76], we took $\sigma = 20$ meters, and we also evaluated the methods with $\sigma = 10\text{m}$ (cf. Table VII). We see that, the LocUNet under the Robustness Scenario outperforms all the ToA ranging-based methods.

Remark 8: We argue that the ToA measurements based on the dominant paths, together with the additional measurement noise we considered, provide a fair, if not favorable, comparison of the performances of the ToA ranging-based methods with that of LocUNet in Robustness Scenario. A more detailed study of the ToA-based methods is, however, beyond the scope of the current paper. We hope that interested researchers would evaluate their ToA-based methods using the presented RadioToASeer Dataset, and improve the state-of-the-art localization performance in realistic urban setting.

E. Comparison with Baselines

To demonstrate the validity of our method, we perform comparisons with baselines. We relate our method to the localization problems (e.g. human/hand pose estimation) in image processing, which can be generally characterized as a so-called *keypoint* regression problem [77]. We describe in the following four approaches, with increasing level of accuracy, where our method falls into the last category. We report our findings based on the numerical experiments we conducted, and discuss the results.

1) *Direct classification*: The problem at hand looks like classification of pixels as occupied by UE or not at first glance. However, the number of classes in this formulation of the problem is prohibitively large (256^2). Furthermore, the flattening of the image and the cross entropy loss used for classification tasks disregard the neighborhood relations of the pixels. Our implementation of this approach did not converge, as expected.

2) *Direct regression*: Another reasonable approach could be the direct regression of the pixel coordinates under a distance based loss, where instead of the CoM layer, a fully connected layer would be used as the last layer. Similar to the direct classification, the flattening at the last layer impairs the spatial generalizability of the network, e.g. the translation equivariance, which is crucial for the localization problem, is lost. Our experiments with this approach didn't converge either. Similar observations were made in many previous works, e.g. in [78].

3) *Heatmap regression*: To preserve the spatial information, the flattening of the layers has to be avoided. Heatmap regression based methods use fully convolutional networks to maintain the spatial information. In such methods, the networks are trained to match the ground truth heatmap, which are usually generated as 2D Gaussian distributions (variance being a hyperparameter to be tuned) centered on the ground truth pixels, and the position is inferred by taking either the pixel with the largest value in the heatmap (in other words, the *mode*, as the heatmap can be interpreted as an a posteriori probability distribution), or the center of mass (i.e., the mean). Hence, these methods are not trained in an end-to-end fashion, i.e., there is a mismatch between the loss function in the training (usually the MSE between the ground truth and the inferred heatmaps) and the actual metric of interest, the Euclidean distance. Our experiments with this approach with the mentioned inference functions (i.e., $\arg \max$ and CoM) have demonstrated worse yet close performances to LocUNet for specific variance values, which are shown in Fig. 5.

4) *Spatial regression*: This approach, which LocUNet is an example of, is based on relying on the heatmaps only as a latent representation, and defining the loss directly on the location coordinates. The inference of the coordinates are achieved by a differentiable function (mostly by CoM as in our paper), which allows end-to-end training. Equipped with the spatial generalization capability thanks to the fully convolutional network, and together with the direct regression of the coordinates, such methods outperform the heatmap regression approach in general [77], [79]–[82].

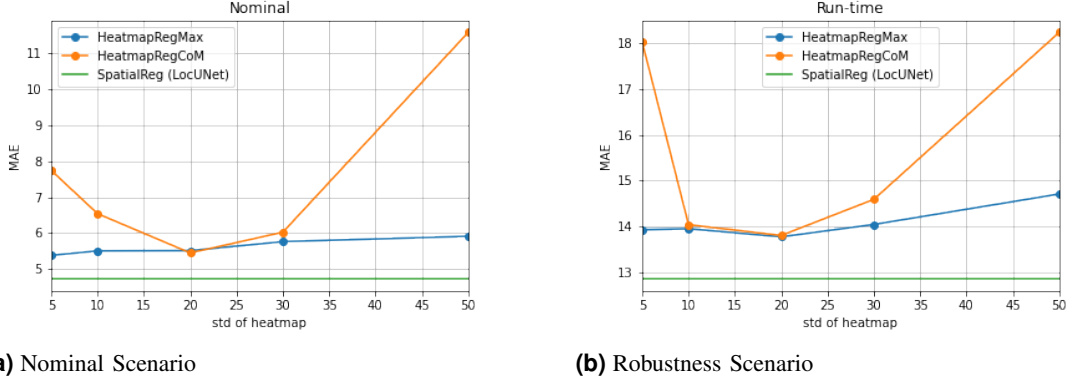


Fig. 5: Heatmap regression vs spatial regression (LocUNet) with varying standard deviation of the ground truth Gaussian heatmaps. Orange and blue curves show the performances of inference by arg max (mode) and CoM (mean), respectively. Constant green line shows the performance of LocUNet.

F. Ablation Study

In this section, we discuss the effectiveness of our neural network design by comparing with other reasonable approaches. In the following, we present the impact of the additional input features (cf. Sec. III-A), the choice of the loss function during the training, and the choice of the last activation function of the network.

1) *Impact of the Additional Input Features*: Our observation is that the impact of the additional input features on the performance is not significant. Hence, for the sake of simplicity of the exposition, throughout the paper we have taken all the additional features as inputs to the LocUNet, when comparisons with other methods are carried out. In Table VIII we show the results of the numerical experiments with (**w**) and without (**w/o**) city (**C**) and Tx (**T**) maps as additional input features.

2) *Impact of the Loss Function in the Training*: We observed that training directly to minimize the loss function with which we validate the accuracy of our method, i.e., the AED (1), performed

better than taking ASED (2) as the loss function (cf. Table VIII). When trained with the ASED loss, we applied the early stopping based on the AED of the validation set, as we observed worse performance when we validated based on the ASED loss. These observations are not surprising, as training directly to optimize the metric of evaluation (when possible), should yield better results, in general. In our experiments with the adopted AED loss, the infinite gradient problem (which would happen when the inferred and the ground-truth values are identical) did not occur, which might have led us to adopt the ASED as the loss function for training.

3) *Impact of the Activation Function Before the CoM Layer:* All of the above mentioned previous works in localization forced the heatmaps by the activation functions to become non-negative, or normalized them to represent a probability distribution (e.g. by Softmax as the activation function). Interestingly, our experiments with several activation functions (ReLU, Softmax, Sigmoid and Leaky ReLU), have shown, that allowing negative values in the heatmap (by using Leaky ReLU as the activation function), performed generally the best among all the activation functions (cf. Table VIII). Here, this quasi-heatmap can be interpreted as a quasi-probability and the CoM as then the mean under a quasi-probability distribution, which is the MMSE estimator (See also the Examples in Sec. IV-B and the *belief/disbelief map* interpretation therein). A study of this interesting observation is, however, beyond the scope of the current paper.

		AED				ASED			
Inputs	# parameters	Leaky ReLu	ReLU	Softmax	Sigmoid	Leaky ReLu	ReLU	Softmax	Sigmoid
wC wT	22,332,381	12.85	n.c.	13.44	13.09	14.35	14.74	15.02	14.27
w/oC wT	22,331,676	12.78	14.30	13.71	13.09	14.53	15.00	15.12	14.17
wC woT	22,328,856	13.47	n.c.	13.56	13.19	14.61	14.69	15.02	14.38
w/oC w/oT	22,328,151	13.04	n.c.	13.74	13.33	14.09	14.65	14.83	14.04

TABLE VIII: Performance of LocUNet with different activation functions at the last layer before CoM, and with different loss functions for training, under different additional input features. n.c.: no convergence.

V. CONCLUSIONS

In this paper we presented a deep learning method to localize a UE based on the measured signal strengths from a set of BSs. Our method, based on the estimates of the true radio maps of each BS, is tailored to work in realistic propagation environments in urban settings. The proposed approach does not necessitate currently uncommon hardware neither at UEs nor at BSs, and does not require an extensive measurement campaign, and thus can be easily integrated in the localization practices that are already in use. Our method outperforms the state-of-the-art

localization algorithms in realistic urban scenarios and enjoys high robustness to inaccuracies in the radio map estimates. We also presented two new datasets, which can be used to evaluate the performances of pathloss fingerprint and ToA ranging-based algorithms in realistic urban environment scenarios.

VI. ACKNOWLEDGMENT

The work presented in this paper was partially funded by the DFG Grant DFG SPP 1798 “Compressed Sensing in Information Processing” through Project Massive MIMO-II, and by the German Ministry for Education and Research as BIFOLD - Berlin Institute for the Foundations of Learning and Data (ref. 01IS18037A).

REFERENCES

- [1] J. Warrior, E. McHenry, and K. McGee, “They know where you are [location detection],” *IEEE Spectrum*, vol. 40, no. 7, pp. 20–25, 2003.
- [2] G. Bresson, Z. Alsayed, L. Yu, and S. Glaser, “Simultaneous localization and mapping: A survey of current trends in autonomous driving,” *IEEE Transactions on Intelligent Vehicles*, vol. 2, no. 3, pp. 194–220, 2017.
- [3] S. Severi, H. Wymeersch, J. Härri, M. Ulmschneider, B. Denis, and M. Bartels, “Beyond GNSS: Highly accurate localization for cooperative-intelligent transport systems,” in *2018 IEEE Wireless Communications and Networking Conference (WCNC)*, 2018, pp. 1–6.
- [4] E. Pournaras, “Proof of witness presence: Blockchain consensus for augmented democracy in smart cities,” *Journal of Parallel and Distributed Computing*, vol. 145, pp. 160–175, 2020.
- [5] R. Di Taranto, S. Muppirisetty, R. Raulefs, D. Slock, T. Svensson, and H. Wymeersch, “Location-aware communications for 5G networks: How location information can improve scalability, latency, and robustness of 5G,” *IEEE Signal Processing Magazine*, vol. 31, no. 6, pp. 102–112, 2014.
- [6] A. H. Sayed, A. Tarighat, and N. Khajehnouri, “Network-based wireless location: Challenges faced in developing techniques for accurate wireless location information,” *IEEE Signal Processing Magazine*, vol. 22, no. 4, pp. 24–40, 2005.
- [7] A. Amini, R. M. Vaghefi, J. M. de la Garza, and R. M. Buehrer, “Improving GPS-based vehicle positioning for intelligent transportation systems,” in *2014 IEEE Intelligent Vehicles Symposium Proceedings*, 2014, pp. 1023–1029.
- [8] I. Guvenc and C. Chong, “A survey on TOA based wireless localization and NLOS mitigation techniques,” *IEEE Communications Surveys Tutorials*, vol. 11, no. 3, pp. 107–124, 2009.
- [9] R. M. Vaghefi and R. M. Buehrer, “Cooperative sensor localization with NLOS mitigation using semidefinite programming,” in *2012 9th Workshop on Positioning, Navigation and Communication*, 2012, pp. 13–18.
- [10] H. Liu, H. Darabi, P. Banerjee, and J. Liu, “Survey of wireless indoor positioning techniques and systems,” *IEEE Transactions on Systems, Man, and Cybernetics, Part C (Applications and Reviews)*, vol. 37, no. 6, pp. 1067–1080, 2007.
- [11] R. M. Vaghefi, M. R. Gholami, and E. G. Ström, “Bearing-only target localization with uncertainties in observer position,” in *2010 IEEE 21st International Symposium on Personal, Indoor and Mobile Radio Communications Workshops*, 2010, pp. 238–242.

- [12] R. M. Vaghefi and R. M. Buehrer, "Received signal strength-based sensor localization in spatially correlated shadowing," in *2013 IEEE International Conference on Acoustics, Speech and Signal Processing*, 2013, pp. 4076–4080.
- [13] H. Laitinen, J. Lahteenmaki, and T. Nordstrom, "Database correlation method for GSM location," in *IEEE VTS 53rd Vehicular Technology Conference, Spring 2001. Proceedings (Cat. No.01CH37202)*, vol. 4, 2001, pp. 2504–2508 vol.4.
- [14] G. Giorgetti, S. Gupta, and G. Manes, "Localization using signal strength: To range or not to range?" in *Proceedings of the First ACM International Workshop on Mobile Entity Localization and Tracking in GPS-Less Environments*, ser. MELT '08. New York, NY, USA: Association for Computing Machinery, 2008, p. 91–96. [Online]. Available: <https://doi.org/10.1145/1410012.1410033>
- [15] A. Karttunen, A. F. Molisch, S. Hur, J. Park, and C. J. Zhang, "Spatially consistent street-by-street path loss model for 28-GHz channels in micro cell urban environments," *IEEE Transactions on Wireless Communications*, vol. 16, no. 11, pp. 7538–7550, 2017.
- [16] S. Maranò, W. M. Gifford, H. Wymeersch, and M. Z. Win, "NLOS identification and mitigation for localization based on UWB experimental data," *IEEE Journal on Selected Areas in Communications*, vol. 28, no. 7, pp. 1026–1035, 2010.
- [17] M. R. Gholami, H. Wymeersch, E. G. Ström, and M. Rydström, "Wireless network positioning as a convex feasibility problem," *EURASIP Journal on Wireless Communications and Networking*, vol. 2011, no. 1, p. 161, 2011.
- [18] A. O. Hero and D. Blatt, "Sensor network source localization via projection onto convex sets (POCS)," in *Proceedings. (ICASSP '05). IEEE International Conference on Acoustics, Speech, and Signal Processing, 2005.*, vol. 3, 2005, pp. iii/689–iii/692 Vol. 3.
- [19] R. M. Vaghefi, J. Schloemann, and R. M. Buehrer, "NLOS mitigation in TOA-based localization using semidefinite programming," in *2013 10th Workshop on Positioning, Navigation and Communication (WPNC)*, Dresden, Germany, 2013, pp. 1–6.
- [20] G. Wang, H. Chen, Y. Li, and N. Ansari, "NLOS error mitigation for TOA-based localization via convex relaxation," *IEEE Transactions on Wireless Communications*, vol. 13, no. 8, pp. 4119–4131, 2014.
- [21] H. Chen, G. Wang, and N. Ansari, "Improved robust TOA-based localization via NLOS balancing parameter estimation," *IEEE Transactions on Vehicular Technology*, vol. 68, no. 6, pp. 6177–6181, 2019.
- [22] S. Tomic, M. Beko, R. Dinis, and P. Montezuma, "A robust bisection-based estimator for TOA-based target localization in NLOS environments," *IEEE Communications Letters*, vol. 21, no. 11, pp. 2488–2491, 2017.
- [23] W. Xiong, C. Schindelhauer, H. Cheung So, and Z. Wang, "Maximum correntropy criterion for robust TOA-based localization in NLOS environments," *arXiv e-prints*, p. arXiv:2009.06032, Sep. 2020.
- [24] Q. D. Vo and P. De, "A survey of fingerprint-based outdoor localization," *IEEE Communications Surveys Tutorials*, vol. 18, no. 1, pp. 491–506, 2016.
- [25] E. Laitinen, J. Talvitie, E.-S. Lohan, and M. Renfors, "Comparison of positioning accuracy of grid and path loss-based mobile positioning methods using received signal strengths," in *Proc. Signal Process. and Appl. Math. for Electron. and Commun. (SPAMEC)*, Cluj-Napoca, Romania, 2011.
- [26] W. Y. Al-Rashdan and A. Tahat, "A comparative performance evaluation of machine learning algorithms for fingerprinting based localization in DM-MIMO wireless systems relying on big data techniques," *IEEE Access*, vol. 8, pp. 109 522–109 534, 2020.
- [27] H. Zou, M. Jin, H. Jiang, L. Xie, and C. J. Spanos, "WinIPS: WiFi-based non-intrusive indoor positioning system with online radio map construction and adaptation," *IEEE Transactions on Wireless Communications*, vol. 16, no. 12, pp. 8118–8130, 2017.
- [28] B. Huang, Z. Xu, B. Jia, and G. Mao, "An online radio map update scheme for WiFi fingerprint-based localization," *IEEE Internet of Things Journal*, vol. 6, no. 4, pp. 6909–6918, 2019.

- [29] K. Rizk, J. F. Wagen, and F. Gardiol, "Two-dimensional ray-tracing modeling for propagation prediction in microcellular environments," *IEEE Trans. Vehic. Tech.*, vol. 46, no. 2, pp. 508–518, May 1997.
- [30] Z. Yun and M. F. Iskander, "Ray tracing for radio propagation modeling: Principles and applications," *IEEE Access*, vol. 3, pp. 1089–1100, 2015.
- [31] R. Hoppe, G. Wölfle, and U. Jakobus, "Wave propagation and radio network planning software WinProp added to the electromagnetic solver package FEKO," in *Proc. Int. Appl. Computational Electromagnetics Society Symp. - Italy (ACES)*, Florence, Italy, March 2017, pp. 1–2.
- [32] A. Del Corte-Valiente, J. M. Gómez-Pulido, O. Gutiérrez-Blanco, and J. L. Castillo-Sequera, "Localization approach based on ray-tracing simulations and fingerprinting techniques for indoor–outdoor scenarios," *Energies*, vol. 12, no. 15, 2019. [Online]. Available: <https://www.mdpi.com/1996-1073/12/15/2943>
- [33] M. Raspopoulos, C. Laoudias, L. Kanaris, A. Kokkinis, C. G. Panayiotou, and S. Stavrou, "3D ray tracing for device-independent fingerprint-based positioning in WLANs," in *2012 9th Workshop on Positioning, Navigation and Communication*, 2012, pp. 109–113.
- [34] P. S. Maher and R. A. Malaney, "A novel fingerprint location method using ray-tracing," in *GLOBECOM 2009 - 2009 IEEE Global Telecommunications Conference*, 2009, pp. 1–5.
- [35] K. El-Kafrawy, M. Youssef, A. El-Keyi, and A. Naguib, "Propagation modeling for accurate indoor WLAN RSS-based localization," in *2010 IEEE 72nd Vehicular Technology Conference - Fall*, 2010, pp. 1–5.
- [36] F. Firdaus, N. A. Ahmad, and S. Sahibuddin, "Accurate indoor-positioning model based on people effect and ray-tracing propagation," *Sensors*, vol. 19, no. 24, 2019.
- [37] M. M. Butt, A. Rao, and D. Yoon, "RF fingerprinting and deep learning assisted UE positioning in 5G," *arXiv preprint arXiv:2001.00977*, 2020.
- [38] G. Wölfle, R. Hoppe, D. Zimmermann, and F. M. Landstorfer, "Enhanced localization technique within urban and indoor environments based on accurate and fast propagation models," in *European Wireless*, Firenze, Italy, February 2002, pp. 3799–3803.
- [39] M. N. de Sousa, R. L. Cardoso, H. S. Melo, J. W. C. Parente, and R. S. Thomä, "Machine learning and multipath fingerprints for emitter localization in urban scenario," in *Developments and Advances in Defense and Security*, Á. Rocha and R. P. Pereira, Eds. Singapore: Springer Singapore, 2020, pp. 217–230.
- [40] R. Levie, C. Yapar, G. Kutyniok, and G. Caire, "RadioUNet: Fast radio map estimation with convolutional neural networks," *IEEE Transactions on Wireless Communications*, vol. 20, no. 6, pp. 4001–4015, 2021.
- [41] D. Li, Y. Lei, H. Zhang, and X. Li, "Outdoor positioning based on deep learning and wireless network fingerprint technology," *International Journal of RF and Microwave Computer-Aided Engineering*, vol. 30, no. 12, p. e22444, 2020.
- [42] K. Elawaad, M. Ezzeldin, and M. Torki, "DeepCReg: Improving cellular-based outdoor localization using CNN-based regressors," in *2020 IEEE Wireless Communications and Networking Conference (WCNC)*, 2020, pp. 1–6.
- [43] P. Garau Burguera, "Logical radio maps for user localization in a real outdoor radio environment," Master's thesis, Aalto University. School of Electrical Engineering, 2020. [Online]. Available: <http://urn.fi/URN:NBN:fi:aalto-2020122056430>
- [44] D. Burghal, A. T. Ravi, V. Rao, A. A. Alghafis, and A. F. Molisch, "A Comprehensive Survey of Machine Learning Based Localization with Wireless Signals," *arXiv e-prints*, p. arXiv:2012.11171, Dec. 2020.
- [45] J. F. Li, Y.-X. Ye, A.-N. Lu, M.-Y. You, K. Huang, and B. Jiang, "Wireless localization based on deep learning: State of art and challenges," *Mathematical Problems in Engineering*, vol. 2020, p. 5214920, 2020.
- [46] E. Javanmardi, Y. Gu, M. Javanmardi, and S. Kamijo, "Autonomous vehicle self-localization based on abstract map and multi-channel LiDAR in urban area," *IATSS Research*, vol. 43, no. 1, pp. 1–13, 2019. [Online]. Available: <https://www.sciencedirect.com/science/article/pii/S038611217301206>

- [47] A. Zaidi, F. Athley, J. Medbo, U. Gustavsson, G. Durisi, and X. Chen, *5G Physical Layer: principles, models and technology components*. Academic Press, 2018.
- [48] R. Hoppe, G. Wölfle, and F. Landstorfer, “Fast 3-D ray tracing for the planning of microcells by intelligent preprocessing of the data base,” in *3rd European Personal and Mobile Communications Conference (EPMCC)*, 1999.
- [49] G. Durgin, N. Patwari, and T. S. Rappaport, “An advanced 3D ray launching method for wireless propagation prediction,” in *1997 IEEE 47th Vehicular Technology Conference. Technology in Motion*, vol. 2, 1997, pp. 785–789 vol.2.
- [50] R. Wahl, G. Wölfle, P. Wertz, P. Wildbolz, and F. Landstorfer, “Dominant path prediction model for urban scenarios,” in *14th IST Mobile and Wireless Communications Summit*, 2005.
- [51] O. Ronneberger, O. Fischer, and T. Brox, “U-Net: Convolutional networks for biomedical image segmentation,” in *Medical Image Computing and Computer-Assisted Intervention – MICCAI 2015*, N. Navab, J. Hornegger, W. M. Wells, and A. F. Frangi, Eds. Cham: Springer International Publishing, 2015, pp. 234–241.
- [52] R. Levie, C. Yapar, G. Kutyniok, and G. Caire, “Pathloss prediction using deep learning with applications to cellular optimization and efficient D2D link scheduling,” in *ICASSP 2020 - 2020 IEEE International Conference on Acoustics, Speech and Signal Processing (ICASSP)*, 2020, pp. 8678–8682.
- [53] “RadioMapSeer Dataset,” <https://RadioMapSeer.github.io/>, 2020, [Online].
- [54] G. Durgin, T. S. Rappaport, and Hao Xu, “Measurements and models for radio path loss and penetration loss in and around homes and trees at 5.85 GHz,” *IEEE Transactions on Communications*, vol. 46, no. 11, pp. 1484–1496, 1998.
- [55] D. P. Kingma and J. Ba, “Adam: A method for stochastic optimization,” in *Proc. Int. Conf. Learn. Represent. (ICLR)*, San Diego, CA, USA, May 2015.
- [56] A. Paszke, S. Gross, F. Massa, A. Lerer, J. Bradbury, G. Chanan, T. Killeen, Z. Lin, N. Gimelshein, L. Antiga, A. Desmaison, A. Kopf, E. Yang, Z. DeVito, M. Raison, A. Tejani, S. Chilamkurthy, B. Steiner, L. Fang, J. Bai, and S. Chintala, “PyTorch: An imperative style, high-performance deep learning library,” in *Advances in Neural Information Processing Systems 32*, H. Wallach, H. Larochelle, A. Beygelzimer, F. d’Alché-Buc, E. Fox, and R. Garnett, Eds. Curran Associates, Inc., 2019, pp. 8024–8035.
- [57] A. Alkhateeb, S. Alex, P. Varkey, Y. Li, Q. Qu, and D. Tujkovic, “Deep learning coordinated beamforming for highly-mobile millimeter wave systems,” *IEEE Access*, vol. 6, pp. 37 328–37 348, 2018.
- [58] A. Alkhateeb, I. Beltagy, and S. Alex, “Machine learning for reliable mmWave systems: Blockage prediction and proactive handoff,” in *2018 IEEE Global Conference on Signal and Information Processing (GlobalSIP)*, 2018, pp. 1055–1059.
- [59] V. Va, J. Choi, T. Shimizu, G. Bansal, and R. W. Heath, “Inverse multipath fingerprinting for millimeter wave V2I beam alignment,” *IEEE Transactions on Vehicular Technology*, vol. 67, no. 5, pp. 4042–4058, 2018.
- [60] M. Alrabeiah, A. Hredzak, and A. Alkhateeb, “Millimeter wave base stations with cameras: Vision-aided beam and blockage prediction,” in *2020 IEEE 91st Vehicular Technology Conference (VTC2020-Spring)*, 2020, pp. 1–5.
- [61] Y. Wang, N. J. Myers, N. González-Prelcic, and R. W. Heath, “Site-specific online compressive beam codebook learning in mmWave vehicular communication,” *IEEE Transactions on Wireless Communications*, vol. 20, no. 5, pp. 3122–3136, 2021.
- [62] S. Chen, Z. Jiang, S. Zhou, Z. Niu, Z. He, A. Marinescu, and L. A. DaSilva, “Learning-based remote channel inference: Feasibility analysis and case study,” *IEEE Transactions on Wireless Communications*, vol. 18, no. 7, pp. 3554–3568, 2019.
- [63] M. S. Sim, Y.-G. Lim, S. H. Park, L. Dai, and C.-B. Chae, “Deep learning-based mmWave beam selection for 5G NR/6G with sub-6 GHz channel information: Algorithms and prototype validation,” *IEEE Access*, vol. 8, pp. 51 634–51 646, 2020.
- [64] M. Khani, M. Alizadeh, J. Hoydis, and P. Fleming, “Adaptive neural signal detection for massive MIMO,” *IEEE Transactions on Wireless Communications*, vol. 19, no. 8, pp. 5635–5648, 2020.

- [65] Y. He, M. Jiang, X. Ling, and C. Zhao, "Robust BICM design for the LDPC Coded DCO-OFDM: A deep learning approach," *IEEE Transactions on Communications*, vol. 68, no. 2, pp. 713–727, 2020.
- [66] H. Ye, G. Y. Li, and B.-H. Juang, "Power of deep learning for channel estimation and signal detection in OFDM systems," *IEEE Wireless Communications Letters*, vol. 7, no. 1, pp. 114–117, 2018.
- [67] J. Guo, C.-K. Wen, S. Jin, and G. Y. Li, "Convolutional neural network-based multiple-rate compressive sensing for massive MIMO CSI feedback: Design, simulation, and analysis," *IEEE Transactions on Wireless Communications*, vol. 19, no. 4, pp. 2827–2840, 2020.
- [68] N. Shlezinger, N. Farsad, Y. C. Eldar, and A. J. Goldsmith, "ViterbiNet: A deep learning based viterbi algorithm for symbol detection," *IEEE Transactions on Wireless Communications*, vol. 19, no. 5, pp. 3319–3331, 2020.
- [69] N. T. Nguyen and K. Lee, "Deep learning-aided tabu search detection for large MIMO systems," *IEEE Transactions on Wireless Communications*, vol. 19, no. 6, pp. 4262–4275, 2020.
- [70] Q. Zhang, Y.-C. Liang, and H. V. Poor, "Intelligent user association for symbiotic radio networks using deep reinforcement learning," *IEEE Transactions on Wireless Communications*, vol. 19, no. 7, pp. 4535–4548, 2020.
- [71] T. Van Luong, Y. Ko, N. A. Vien, M. Matthaiou, and H. Q. Ngo, "Deep energy autoencoder for noncoherent multicarrier MU-SIMO systems," *IEEE Transactions on Wireless Communications*, vol. 19, no. 6, pp. 3952–3962, 2020.
- [72] J. Gou, B. Yu, S. J. Maybank, and D. Tao, "Knowledge distillation: A survey," *International Journal of Computer Vision*, vol. 129, no. 6, pp. 1789–1819, 2021.
- [73] OpenStreetMap contributors, "Planet dump retrieved from <https://planet.osm.org> ," <https://www.openstreetmap.org>, 2017.
- [74] P. Bahl and V. N. Padmanabhan, "RADAR: An in-building RF-based user location and tracking system," in *Proceedings IEEE INFOCOM 2000. Conference on Computer Communications. Nineteenth Annual Joint Conference of the IEEE Computer and Communications Societies (Cat. No.00CH37064)*, vol. 2, 2000, pp. 775–784 vol.2.
- [75] J. Oh and J. Kim, "Adaptive k-nearest neighbour algorithm for WiFi fingerprint positioning," *ICT Express*, vol. 4, no. 2, pp. 91 – 94, 2018, sI on Artificial Intelligence and Machine Learning. [Online]. Available: <http://www.sciencedirect.com/science/article/pii/S240595951830050X>
- [76] F. Pérez-Cruz, P. M. Olmos, M. M. Zhang, and H. Huang, "Probabilistic time of arrival localization," *IEEE Signal Processing Letters*, vol. 26, no. 11, pp. 1683–1687, 2019.
- [77] C. Tensmeyer and T. Martinez, "Robust keypoint detection," in *2019 International Conference on Document Analysis and Recognition Workshops (ICDARW)*, vol. 5, 2019, pp. 1–7.
- [78] B. Brousseau, J. Rose, and M. Eizenman, "Hybrid eye-tracking on a smartphone with CNN feature extraction and an infrared 3D model," *Sensors*, vol. 20, no. 2, 2020. [Online]. Available: <https://www.mdpi.com/1424-8220/20/2/543>
- [79] A. Nibali, Z. He, S. Morgan, and L. Prendergast, "Numerical coordinate regression with convolutional neural networks," *arXiv preprint arXiv:1801.07372*, 2018.
- [80] J. P. Robinson, Y. Li, N. Zhang, Y. Fu, and S. Tulyakov, "Laplace landmark localization," in *2019 IEEE/CVF International Conference on Computer Vision (ICCV)*, 2019, pp. 10 102–10 111.
- [81] X. Sun, B. Xiao, F. Wei, S. Liang, and Y. Wei, "Integral human pose regression," in *Proceedings of the European Conference on Computer Vision (ECCV)*, September 2018.
- [82] D. C. Luvizon, H. Tabia, and D. Picard, "Human pose regression by combining indirect part detection and contextual information," *Computers & Graphics*, vol. 85, pp. 15–22, 2019.